atmosphere

MDPI

Article

Investigating Meteorological Factors Influencing Pollutant Concentrations and Copernicus Atmosphere Monitoring Service (CAMS) Model Forecasts in the Tehran Metropolis

Sara Karami [1], Zahra Ghassabi [2], Noushin Khoddam [3] and Maral Habibi [4,*]

[1] Research Institute of Meteorology and Atmospheric Sciences, Department of Air Pollution and Dust, Tehran 14977-16385, Iran; karamis.62@gmail.com
[2] Research Institute of Meteorology and Atmospheric Sciences, Department of Atmospheric Hazard Forecast, Tehran 14977-16385, Iran; z.ghassabi@gmail.com
[3] International Center for Dust Studies, Research Institute of Meteorology and Atmospheric Sciences, Tehran 14977-16385, Iran; noushin_khoddam@ut.ac.ir
[4] Department of Geography and Regional Sciences, University of Graz, A-8010 Graz, Austria
* Correspondence: maral.habibi@uni-graz.at

Abstract: In recent years, air pollution has become a significant issue for megacities. This study analyzed the air pollution levels in Tehran and the relationship between pollutant concentrations and atmospheric quantities during 2023. The correlation coefficients between wind speed, temperature, mean sea level pressure (MSLP), and relative humidity (RH) were calculated against the concentrations of NO_2, NO_x, PM_{10}, and $PM_{2.5}$. Additionally, one case study was conducted for each pollutant. Approximately 72% of haze phenomena in Tehran were recorded in November, December, and January. The monthly pattern of PM_{10} concentration indicated higher levels in the southern and western parts of Tehran. For $PM_{2.5}$, in addition to these areas, significant concentrations were also observed in the central and eastern parts. NO_2 concentrations were found to be higher in the northeast and northern areas. An inverse relationship was found between wind speed and temperature with pollutant concentrations. Positive correlations between MSLP and pollutant concentrations suggested that the pollutant levels also increased as air pressure rose. RH showed a significant direct relationship with $PM_{2.5}$ and NO_x. Synoptic analysis revealed that PM_{10} case studies often occurred during the warm season, with a thermal low pressure situated over the Iranian plateau. During $PM_{2.5}$ and NO_2 pollution events, Tehran was influenced by high pressure, and 10 m wind speeds were weak. Finally, verification of the 24 h forecast of the CAMS model showed that, while the model accurately predicted the spatial distribution of pollutants in most cases, it consistently underestimated the concentration levels.

Keywords: pollutant concentrations; atmospheric conditions; cams model; Tehran metropolis

check for updates

Academic Editors: Yu Zhao and Yunhua Chang

Received: 6 January 2025
Revised: 13 February 2025
Accepted: 21 February 2025
Published: 24 February 2025

Citation: Karami, S.; Ghassabi, Z.; Khoddam, N.; Habibi, M. Investigating Meteorological Factors Influencing Pollutant Concentrations and Copernicus Atmosphere Monitoring Service (CAMS) Model Forecasts in the Tehran Metropolis. *Atmosphere* **2025**, *16*, 264. https://doi.org/10.3390/atmos16030264

Copyright: © 2025 by the authors. Licensee MDPI, Basel, Switzerland. This article is an open access article distributed under the terms and conditions of the Creative Commons Attribution (CC BY) license (https://creativecommons.org/licenses/by/4.0/).

1. Introduction

Rapid industrialization in developing countries has led to a significant rise in air pollution, which has emerged as one of the most critical environmental challenges that these nations face [1–3]. This growing pollution crisis severely threatens both environmental and human health. Numerous studies have linked air pollution to an increased risk of acute and chronic diseases, including cardiovascular, respiratory, and pulmonary disorders, as well as cancer [4–7]. Air pollution substantially drives climate change [8,9]. Aerosols can influence the Earth's energy balance by reflecting or absorbing sunlight, leading to either cooling

or warming effects, depending on their composition and interaction with clouds [10–12]. Furthermore, air pollutants can affect cultural heritage building materials [13] and cause socio-economic damage [14].

Meteorological factors, including wind speed, temperature, humidity, and precipitation, play a crucial role in determining air pollutants' dispersion, accumulation, and chemical transformation [15–18]. Stable atmospheric conditions, such as temperature inversions, can trap pollutants near the Earth's surface, leading to elevated pollution levels [19,20]. In contrast, strong winds can disperse pollutants, reducing their concentration in localized areas [21]. The influence of meteorological factors on air pollution highlights the need for an integrated understanding of atmospheric conditions and pollution sources in order to manage air quality in megacities effectively [22,23].

Accurately predicting air pollution events is critical for mitigating their harmful effects on public health and the environment. Early warnings can help to minimize economic losses and reduce mortality rates associated with high pollution episodes [24]. Identifying synoptic weather patterns associated with severe pollution events is essential for improving predictive models [25,26]. Machine learning methods have been widely used in air pollution prediction in recent years, e.g., [27–29]. Numerical air pollution models, widely used in urban areas globally, have become indispensable tools for managing air quality [30,31]. Despite recent advancements, these models require further refinement to improve their quantitative accuracy, particularly in complex urban environments [32,33].

In Iran, the increase in air pollution has been particularly pronounced since the onset of industrialization in the 1970s. In major cities such as Tehran, Mashhad, Tabriz, Isfahan, Ahvaz, Arak, and Karaj, pollution levels have reached hazardous thresholds in recent decades [34]. A study showed that Tehran's daily air quality index (AQI) increased by 11.8% in 11 years (2002–2012) [35]. Another study by Faraji et al. [36] identified primary and secondary factors contributing to air pollution in Tehran. Primary factors include natural sources, fossil fuel consumption, industrial factory emissions, and traffic congestion. Secondary factors encompass population density, industrial expansion, residential heating and cooling systems, limited green spaces, and poor waste management practices. The rapid growth of urbanization and inefficient infrastructure have further exacerbated the problem [37].

Both industrial and meteorological–climatic factors contribute to air pollution in Tehran [38,39]. Changes in temperature, precipitation, pressure, and wind affect the levels of air pollution in the city [40,41]. In addition to meteorological factors, human activities, and geographical conditions, such as Tehran's topography, also play a significant role in air pollution [42].

This study aims to investigate the air pollution levels in Tehran during 2023, a year in which the frequency of pollution incidents significantly increased compared to previous years. It also examines the atmospheric factors influencing these pollution events, focusing on case studies of different pollutants. Additionally, the study evaluates the qualitative performance of the Copernicus Atmosphere Monitoring Service (CAMS) model in forecasting pollution levels during these events, to improve forecast capabilities for future air quality management.

2. Material and Methods

2.1. Study Area

Figure 1 shows the city of Tehran and its 22 districts, along with the location of synoptic meteorological stations and air pollution monitoring stations. Among the stations, the Mehrabad Airport synoptic station, which has the most complete data in the studied time (year 2023), was selected to investigate meteorological quantities. Shadabad air pollution

monitoring station, located in the 18th district of Tehran, is the closest station to the Mehrabad station, which has complete data to check the concentration of PM_{10}, $PM_{2.5}$, and NO_2 pollutants, and their relationship with the meteorological quantities was considered.

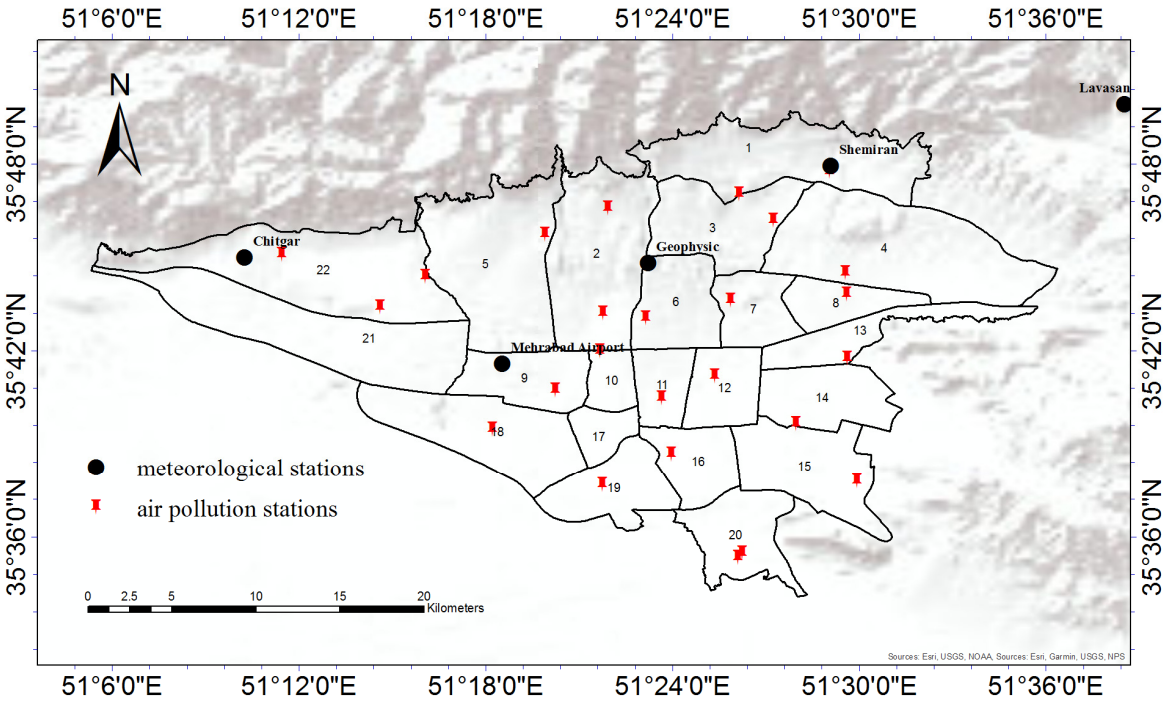

Figure 1. The study area and locations of synoptic and air pollution stations.

2.2. Data

2.2.1. Meteorological Data

The meteorological data included the quantities of phenomenon code, horizontal visibility, wind speed and direction, temperature, MSLP, and RH from the synoptic weather station of Mehrabad Airport in Tehran, reported 8 times a day, over 3 h, at 00, 03, 06, 09, 12, 15, 18 and 21 UTC. These data were taken from the Iran Meteorological Organization (IRIMO).

To perform synoptic analysis and draw the SKEW-T diagram at Mehrabad Airport's position, ERA5 reanalysis data with a 0.25 degrees horizontal resolution, available from https://cds.climate.copernicus.eu (accessed on 26 February 2024), was used. These data include MSLP and wind velocity at 10 m height, geopotential height at 850 hPa, RH at 700 hPa, geopotential height at 500 hPa level, temperature, RH, and wind velocity from 1000 to 100 hPa levels.

2.2.2. Air Pollution Data

Air pollution data include concentrations of O_3, NO, NO_2, NO_x, SO_2, PM_{10}, and $PM_{2.5}$ pollutants from air quality monitoring stations in Tehran city, which are reported in one-hour intervals and in local time. These data were taken from the website of the Tehran Air Quality Control Company affiliated with the Tehran Municipality: https://airnow.tehran.ir (accessed on 13 January 2024). Since these data are quality controlled, there was no need to carry out anything in this regard. Only for comparison with the meteorological data and model output, their time was converted from local time to UTC, and given that the concentration of some pollutants is reported as ppb, all units were converted to standard units (WHO, 2010).

2.3. Methodology

One of the phenomena that indicates the presence of air pollution in the atmosphere is the phenomenon of haze, which is shown in meteorological reports from synoptic stations with the code 05. According to the definition of the World Meteorological Organization (WMO), the definition of haze is "A suspension in the air of extremely small, dry particles invisible to the naked eye and sufficiently numerous to give the air an opalescent appearance". In this study, firstly, to investigate the number of hazy days in Tehran city in 2023, the monthly frequency of the presence of weather code 05 was investigated at Mehrabad Airport meteorological station. To determine the occurrence time of the most haze phenomena, the frequency of code 05 at different hours of the day in different months of this year was also investigated at Mehrabad station. Since wind speed plays an important role in air pollution, the monthly average wind speed was also checked at this meteorological station.

Subsequently, the monthly average pollutant concentration was checked using the data from the Shadabad air pollution monitoring station, which is close to the Mehrabad meteorological station, and has a complete data set. Then, the concentrations of the three pollutants PM_{10}, $PM_{2.5}$, and NO_2 at different hours of the day, in each month of 2023, were investigated at this station. Since $PM_{2.5}$ is both a primary and a secondary pollutant that is produced from the conversion of the gaseous pollutants NO_x and SO_2, scatter diagrams of $PM_{2.5}$, NO_x, and SO_2 concentrations in January, November, and December, which had the highest amount of $PM_{2.5}$, were created. Considering that surface ozone (O_3) is a secondary pollutant produced by the effect of the sun's ultraviolet rays on nitrogen oxides, the relationship between NO_x and O_3 concentrations in the months with the highest average NO_x concentrations (January and September to December) was analyzed. Although O_3 can be fumigated by vertical turbulence from the free troposphere, this process is not analyzed here.

To investigate the effect of different factors on the amount of visibility in Tehran, the correlations of horizontal visibility with wind speed, temperature, mean sea level pressure (MSLP), and relative humidity (RH) at Mehrabad station, and also with the concentrations of O_3, nitric oxide (NO), NO_2, NO_x, SO_2, PM_{10}, and $PM_{2.5}$ at Shadabad station, in different months of 2023, along with their significant levels, were investigated.

To study the monthly pattern of air pollution in Tehran city, a monthly average concentration map of the PM_{10}, $PM_{2.5}$, and NO_2 pollutants, using the data of the monitoring stations in the city and using the inverse distance weighting interpolation method (IDW), was shown for 2023. In order to investigate the factors that affect the pollutant distribution pattern in Tehran, the emission rates of pollutants from different parts of the city, and the effects of atmospheric quantities on the concentrations of pollutants, were investigated. An annual emission map of nitrogen oxides and particulate matter (PM) in 2013, on a grid with a 500 m resolution, was created from the air quality report of Tehran, prepared in 2016 by the Air Quality Control Company affiliated with the Tehran Municipality (https://air.tehran.ir/ (accessed on 16 January 2024)). In order to analyze the impact of atmospheric quantities, the correlation coefficients of pollutant concentration with meteorological quantities of wind speed, temperature, MSLP, and RH, and their significance levels, were determined.

Next, to further investigate the air pollution in Tehran city, one case of air pollution caused by each of the PM_{10}, $PM_{2.5}$, and NO_2 pollutants was investigated. For each case study, the time series of the responsible pollutant concentration from the Shadabad air pollution station, and the horizontal visibility and RH from the Mehrabad Airport meteorological station, were provided. Also, maps of MSLP and wind velocity at 10 m height, geopotential height, wind velocity at the 850 hPa level, RH and stream lines at the 700 hPa level, geopotential height at the 500 hPa level, and a SKEW-T diagram of the position of the Mehrabad station with ERA5 data, with a horizontal resolution of 0.25 degrees, were

presented to determine the prevailing weather conditions over the region at the time of occurrence of each episode. Finally, to verify the feasibility of pollutant concentration forecasting, the 24 h forecast of the CAMS model was compared with the concentration patterns obtained from the air pollution monitoring stations in Tehran.

CAMS Model

The CAMS model developed by ECMWF provides daily global and regional (over Europe) air quality forecasts. The model used in the CAMS global atmospheric composition forecast is the Integrated Forecast System (IFS), which also produces ECMWF weather forecasts, but with additional modules enabled for particulate matter, reactive gasses, and greenhouse gasses. CAMS represents a five-day global forecast of atmospheric composition twice a day (at 00:00 and 12:00 UTC). For more information about this model, refer to [43].

3. Discussion and Results

3.1. Mehrabad Airport Synoptic Station Data

Figure 2a shows the percentage frequency of the presence of weather code 05 at Mehrabad Airport synoptic station during 2023. A total of 2918 records were taken eight times a day over 364 days, of which 590 records (about 20%) were attributed to weather code 05. The highest frequency of code 05 (26%) occurred in January, followed by December (25%) and November (21%); in total, 72% of code 05 observations were recorded during November, December, and January.

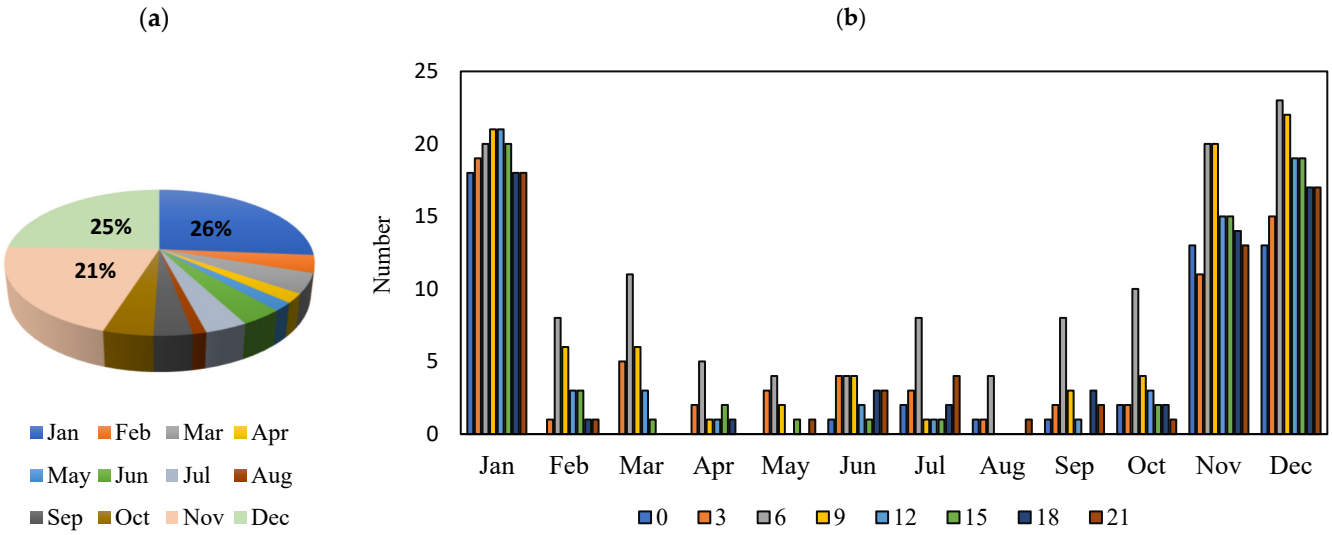

Figure 2. (**a**) The monthly frequency percentage of code 05 and (**b**) the monthly frequency number of code 05 at different hours of the day at the Mehrabad Airport station, 2023.

Figure 2b illustrates the frequency of code 05 at different hours of the day for each month at Mehrabad station. The highest occurrence of haze was observed at 06 UTC in nearly all months. In Tehran, many vehicles are active in the city due to office and school opening hours around this time, leading to increased emissions and higher air pollution levels. Additionally, factors such as temperature inversions, calm winds, and higher humidity in the early morning hours contributed to the occurrence of haze in the Tehran metropolis [44]. In January, November, and December—when code 05 records were most frequent—the number of records across different hours was smaller, with January showing the slightest variation.

Figure 3a illustrates the hourly average wind speed at the Mehrabad station for 2023. The highest average wind speed was recorded at 12 UTC, while the lowest occurred at

03 UTC. The monthly average wind speeds at different hours of the day are displayed in Figure 3b. The lowest wind speeds corresponded to December, November, and January, respectively, while the highest wind speeds were recorded in May, April, and June, respectively. Thus, the months with the highest frequency of haze coincided with the lowest average wind speeds. The highest average wind speed was recorded at 12 UTC in most months. However, wind speeds at 09 UTC were slightly higher than at 12 UTC in February, August, and September. Additionally, wind speeds at 15 UTC were also notable from April to August.

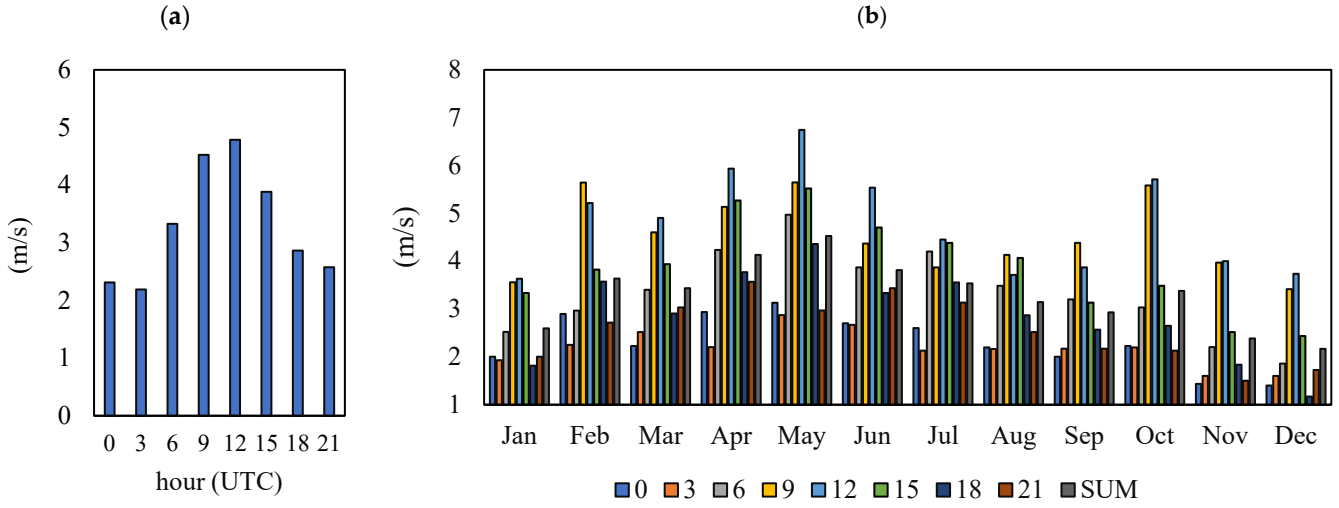

Figure 3. (**a**) The hourly and (**b**) monthly average wind speeds at the Mehrabad station at different hours of the day, 2023.

In a study by Pegahfar et al. [45], the diurnal wind pattern in Tehran was investigated. The results showed that during the day, the prevailing wind is southwesterly (anabatic wind), and at night, northeasterly (nocturnal katabatic wind). In the middle hours of the day, which show the highest wind speed, especially in the summer season and in the absence of strong synoptic systems, the southerly wind blowing from the plain to the mountains is clearly visible, due to the presence of high altitudes in northern Tehran.

3.2. Shadabad Air Pollution Monitoring Station Data

Figure 4 shows the monthly average concentration of pollutants at Shadabad station in 2023. The maximum O_3 concentration was observed in June, August, and July, respectively. The highest NO concentrations were recorded in December, November, and January, while NO_2 concentrations peaked in May, June, and December. For NO_x, the highest levels were observed in December, January, and November. Similarly, January and December recorded the highest concentrations of SO_2. The maximum concentration of PM_{10} was recorded in July, September, and August, while $PM_{2.5}$ concentrations peaked in January, December, and November. The highest $PM_{2.5}$ levels occurred during months with elevated concentrations of NO_x and SO_2, likely due to the formation of secondary pollutants.

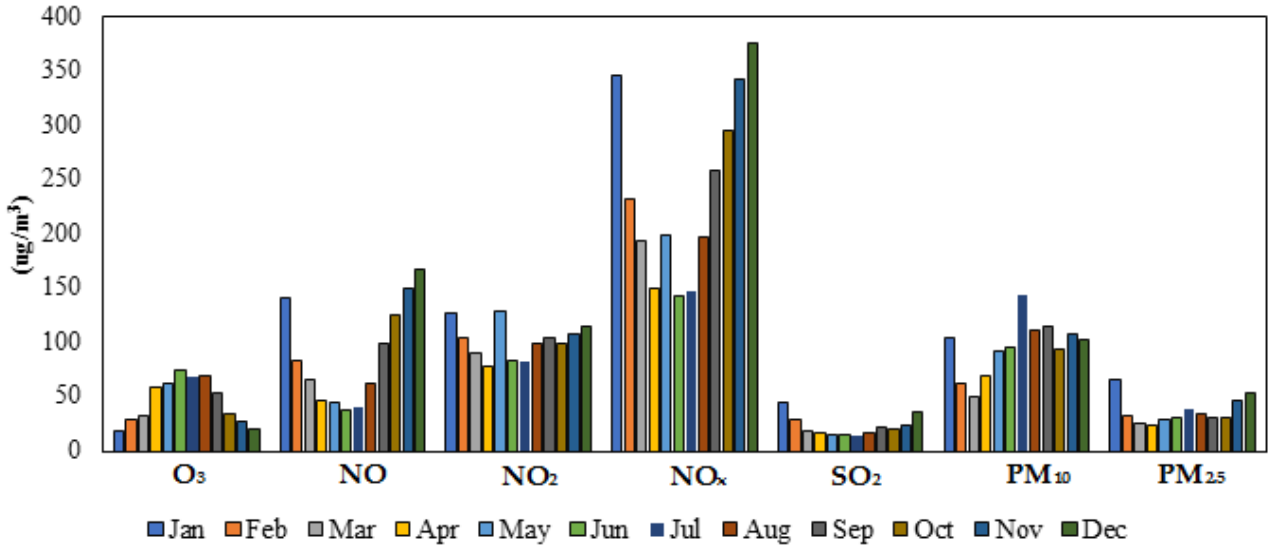

Figure 4. The monthly average concentration of pollutants at the Shadabad station, 2023.

3.3. The Monthly Average Concentration of Pollutants at Different Hours of the Day

3.3.1. PM_{10} Pollutant

Figure 5 illustrates the monthly average concentration of PM_{10} at different hours of the day in 2023. During July, August, and September—when PM_{10} concentrations were highest—the peak levels were recorded at 21 and 00 UTC, coinciding with the boundary layer's low height and a stable nocturnal boundary layer. Many studies have shown that the height of the boundary layer has a significant effect on the concentration of pollutants e.g., [46–48].

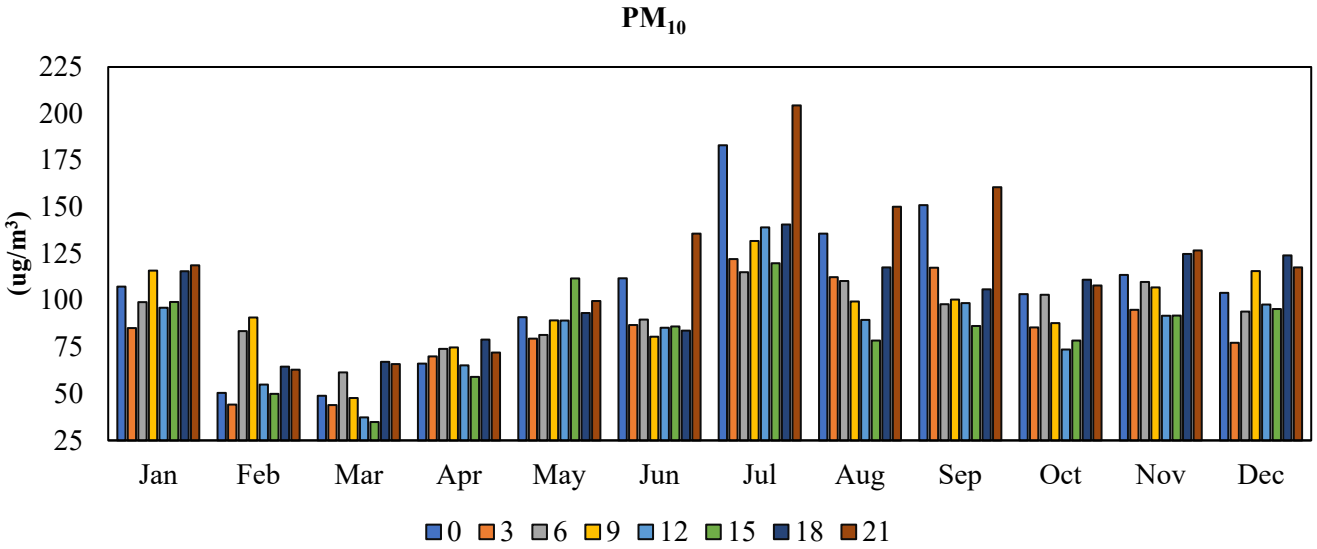

Figure 5. The monthly average PM_{10} concentration at different hours of the day in the year 2023.

A comparison of $PM_{2.5}$ and PM_{10} concentrations reveals that in November, December, and January, approximately half of the PM_{10} concentration was attributable to particles with a diameter of less than 2.5 μm. In contrast, this proportion dropped to less than one-third during July, August, and September. In the warmer months, a significant portion of PM_{10} originated from dust particles with larger diameters from both local and non-local sources [49]. Therefore, $PM_{2.5}$ particles with smaller diameters constituted only a small fraction of the PM_{10} concentration.

3.3.2. $PM_{2.5}$ Pollutant

Figure 6 shows the monthly average concentration of $PM_{2.5}$ at different hours of the day in 2023. In January, when the highest concentration of $PM_{2.5}$ was observed, peak concentrations occurred at 21, 00, 18, and 09 UTC, respectively. The increase in concentration at 18:00, 21:00, and 00:00 was due to the formation of a stable nocturnal boundary layer, which limited vertical mixing and led to higher surface concentrations of pollutants [50]. At 09 UTC, $PM_{2.5}$ levels rose due to increased transportation and traffic associated with schools and offices opening. A time series analysis of $PM_{2.5}$ concentrations in Dhaka city from 2016 to 2023 showed that the opening and closing times of offices and schools had a significant impact on the concentration of this pollutant [51]. In December, the hours of maximum concentration were 18, 09, 21, and 00 UTC, while in November, they were 21, 18, 06, 09, and 00 UTC, respectively. During the warmer months, the highest $PM_{2.5}$ concentration was recorded in July, at 21 UTC. In this month, higher daytime temperatures and an increased boundary layer height resulted in a more pronounced concentration difference between night-time and day-time hours [52].

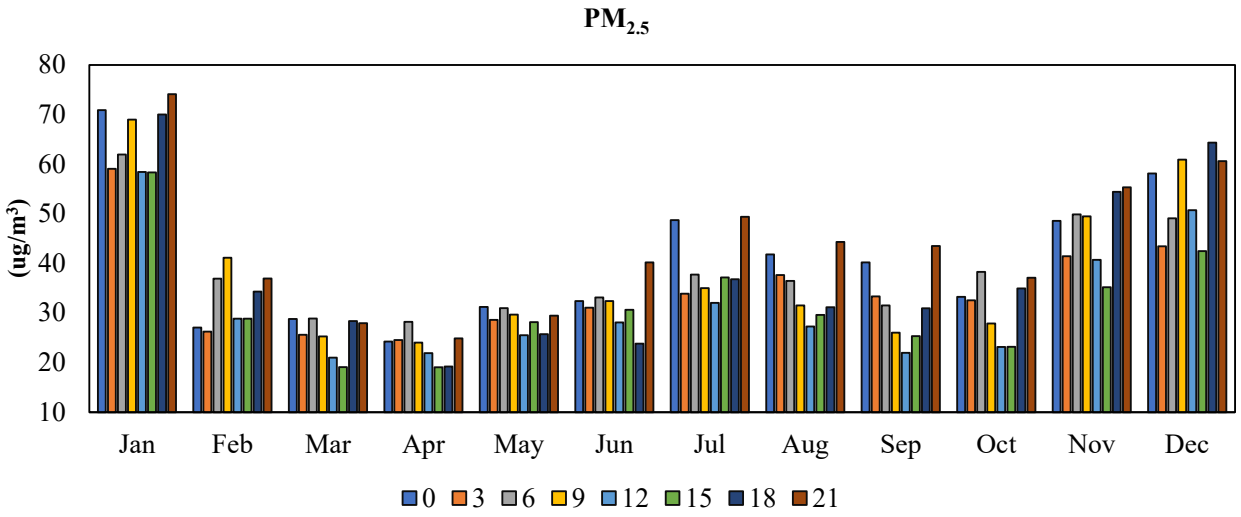

Figure 6. The monthly average $PM_{2.5}$ concentration at different hours of the day of 2023.

Since $PM_{2.5}$ acts as both a primary and secondary pollutant formed through the conversion of gaseous pollutants like NO_x and SO_2, Table 1 presents the correlations and R-squared values between the NO_x, SO_2, and $PM_{2.5}$ concentrations for January, November, and December 2023—the months with the highest $PM_{2.5}$ levels. The scatterplots reveal that high $PM_{2.5}$ concentrations coincided with elevated NO_x and SO_2 levels, highlighting the role of these pollutants in the formation of secondary $PM_{2.5}$. High NO_x and SO_2 concentrations during these months suggest their involvement in chemical processes that generate secondary particles via oxidation [53]. However, a significant portion of $PM_{2.5}$ in the Tehran metropolis originates as a primary pollutant, directly entering the atmosphere through fuel combustion in vehicles, industrial activities, and dust from local and predominantly non-local sources, especially during the warmer months of the year [54].

Table 1. Correlations and R-squared values between NO_x, SO_2, and $PM_{2.5}$ concentrations in January, November, and December 2023.

	R	**R^2**
NO_x and $PM_{2.5}$	0.4844	0.2347
SO_2 and $PM_{2.5}$	0.4842	0.2345

3.3.3. NO_2 Pollutant

The monthly average concentration of NO_2 at different hours of the day in 2023 is shown in Figure 7. The highest concentration was recorded in December at 06, 18, and 21 UTC, followed by November, with peak concentrations at 18, 21, and 06 UTC, and October, with peaks at 21, 00, and 18 UTC. During these months, the combination of lower temperatures, a reduced boundary layer height, and an increased likelihood of stable weather conditions amplified the impact of daily traffic on pollutant concentrations.

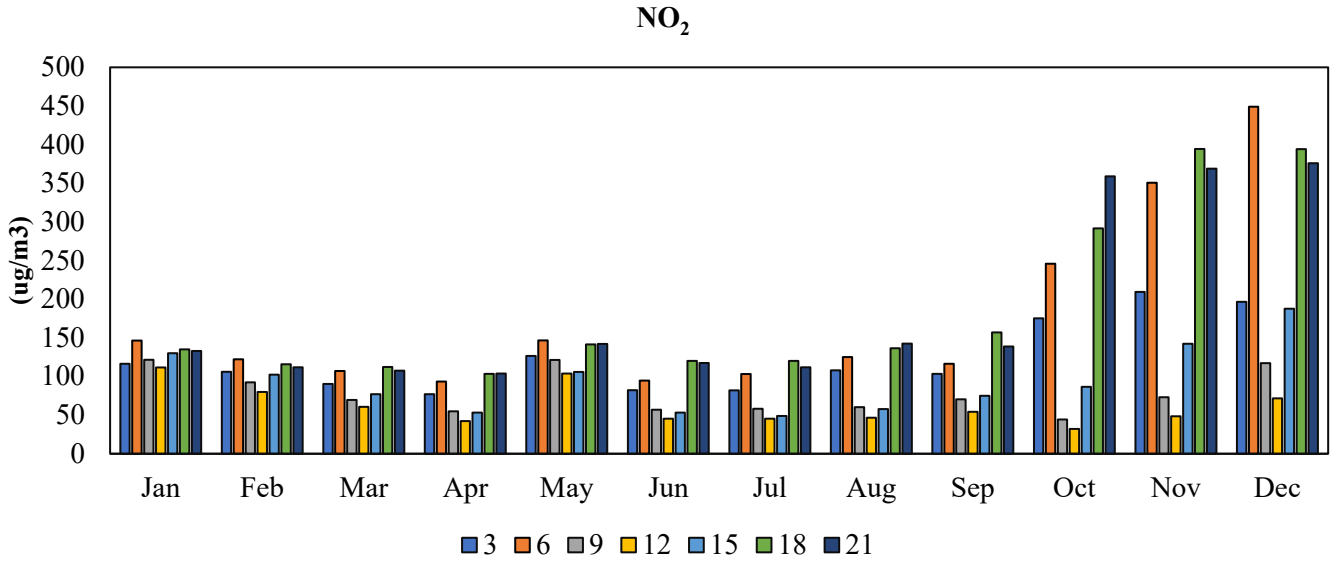

Figure 7. The monthly average NO_2 concentration at different hours of the day in 2023.

Table 2 shows the correlations and R-squared values between the NO_2, NO_x, and O_3 concentrations for January and the months from September to December, which had the highest NO_x levels. The data demonstrate a strong inverse relationship between the O_3 and NO_x concentrations, indicating the formation of secondary O_3 from NO_x. As O_3 forms, NO_x levels decrease significantly, due to chemical reactions that consume NO_x and convert it into O_3. A complete explanation for the relationship between tropospheric ozone and NO_x can be found in [55].

Table 2. Correlations and R-squared values between NO_2, NO_x, and O_3 concentrations in the months of January and September to December 2023.

	R	**R^2**
NO_2 and O_3	−0.493	0.243
NO_x and O_3	−0.486	0.236

Similarly, the relationship between O_3 and NO_2 concentrations shows an inverse relationship, but with a gentler value, which can be attributed to the production of NO_2 from O_3 through a feedback process, which increases O_3 concentrations and, consequently, NO_2 levels. A mechanism known as O_3 titration also contributes to this dynamic: O_3 reacts with NO to form NO_2, regenerating NO_2 and slightly raising its concentration.

In summary, these values highlight the complex interactions between these pollutants. NO_x serves as a key precursor for O_3 production, with its reduction driving O_3 formation. At the same time, the interplay between O_3 and NO_2 reflects a feedback loop, where these pollutants evolve together and reinforce each other's presence in the atmosphere.

3.4. The Effect of Some Meteorological Quantities and Pollutant Concentrations on the Occurrence of Haze and Horizontal Visibility Reduction

Table 3 presents the correlations of horizontal visibility with wind speed, temperature, MSLP, and RH at the Mehrabad station during 2023, precisely when weather code 05 was recorded. Additionally, it shows the correlations of horizontal visibility at the Mehrabad station with the concentrations of O_3, NO, NO_2, NO_x, SO_2, PM_{10}, and $PM_{2.5}$ at the Shadabad station. Values marked with one star (*) are significant at the 5% level, while those with two stars (**) are significant at the 1% level.

Table 3. Correlations between some meteorological quantities at the Mehrabad station and pollutant concentrations at the Shadabad station in the months of 2023 and at the time that code 05 was reported.

Month	Wind	Temp	MSLP	RH	O_3	NO	NO_2	NO_x	SO_2	PM_{10}	$PM_{2.5}$
Jan	0.08	−0.18	−0.30 *	0.07	−0.07	−0.14	−0.39 **	−0.18	−0.14	−0.47 **	−0.53 **
Feb	−0.08	0.81 **	0.28	−0.90 **	0.15	−0.03	−0.45 *	−0.10	−0.63 **	−0.26	−0.77 **
Mar	0.31	−0.06	0.39 *	−0.10	0.28	0.21	0.19	0.21	0.02	0.29	0.11
Apr	−0.38	0.25	−0.03	−0.27	0.28	−0.24	−0.14	−0.24	−0.09	0.16	−0.09
May	0.73 **	0.47	−0.16	−0.79 **	0.20	−0.29	0.19	−0.12	0.25	−0.14	−0.30
Jun	0.16	0.17	0.26	−0.16	0.13	−0.22	−0.26	−0.25	−0.17	−0.14	−0.04
Jul	0.15	0.29	0.46 *	−0.23	−0.08	−0.18	−0.09	−0.18	−0.01	−0.25	−0.31
Aug	−0.32	0.32	−0.30	−0.41	0.96 **	−0.37	−0.27	−0.35	0.52	−0.21	−0.06
Sep	0.05	0.05	−0.15	−0.17	−0.03	−0.21	0.09	−0.16	0.00	−0.17	−0.11
Oct	0.02	0.10	0.14	−0.27	−0.07	0.18	0.03	0.16	0.25	0.18	−0.13
Nov	−0.07	−0.05	0.32 **	0.21*	−0.09	−0.05	−0.39 **	−0.10	−0.38 **	−0.24 **	−0.51 **
Dec	0.13	−0.33 **	−0.02	0.28 **	−0.11	−0.11	−0.40 **	−0.17 *	−0.19 *	−0.41 **	−0.49 **
total	0.15 **	0.51 **	−0.38 **	−0.30 **	0.12 **	−0.20 **	−0.44 **	−0.25 **	−0.41 **	−0.15 **	−0.63 **

* Significant at the 5% level. ** Significant at the 1% level.

The analysis reveals that horizontal visibility significantly correlated with the studied variables at the 1% confidence level. Visibility was positively associated with wind speed, temperature, and O_3 concentration, and negatively associated with MSLP, RH, and pollutant concentrations. The cold months of the year showed stronger and more significant correlations, indicating a greater impact of these variables on visibility during this period.

3.5. Monthly Average Concentrations of Pollutants in the City of Tehran

3.5.1. PM_{10} Pollutant

Figure 8 shows the monthly average concentration of PM_{10} in 2023 in Tehran, using data from pollution monitoring stations. The highest concentration of PM_{10} was in July. In this month, the concentration of PM_{10} was significant in almost the entire city, caused by the entrance of dust from sources around Tehran or other areas inside and outside the country [56]; the lowest concentration of PM_{10} was recorded March and April. The increase in the height of the boundary layer compared to the cold months of the year, and, on the other hand, the decrease in the activity of dust sources due to more precipitation and soil moisture compared to the warm months, caused a decrease in the concentration of PM_{10} in these two months in Tehran [57]. In general, the concentration of PM_{10} was higher in the south and west of Tehran, because most of the dust sources that affect this city, especially in the warm seasons, are located in the south and west of Tehran.

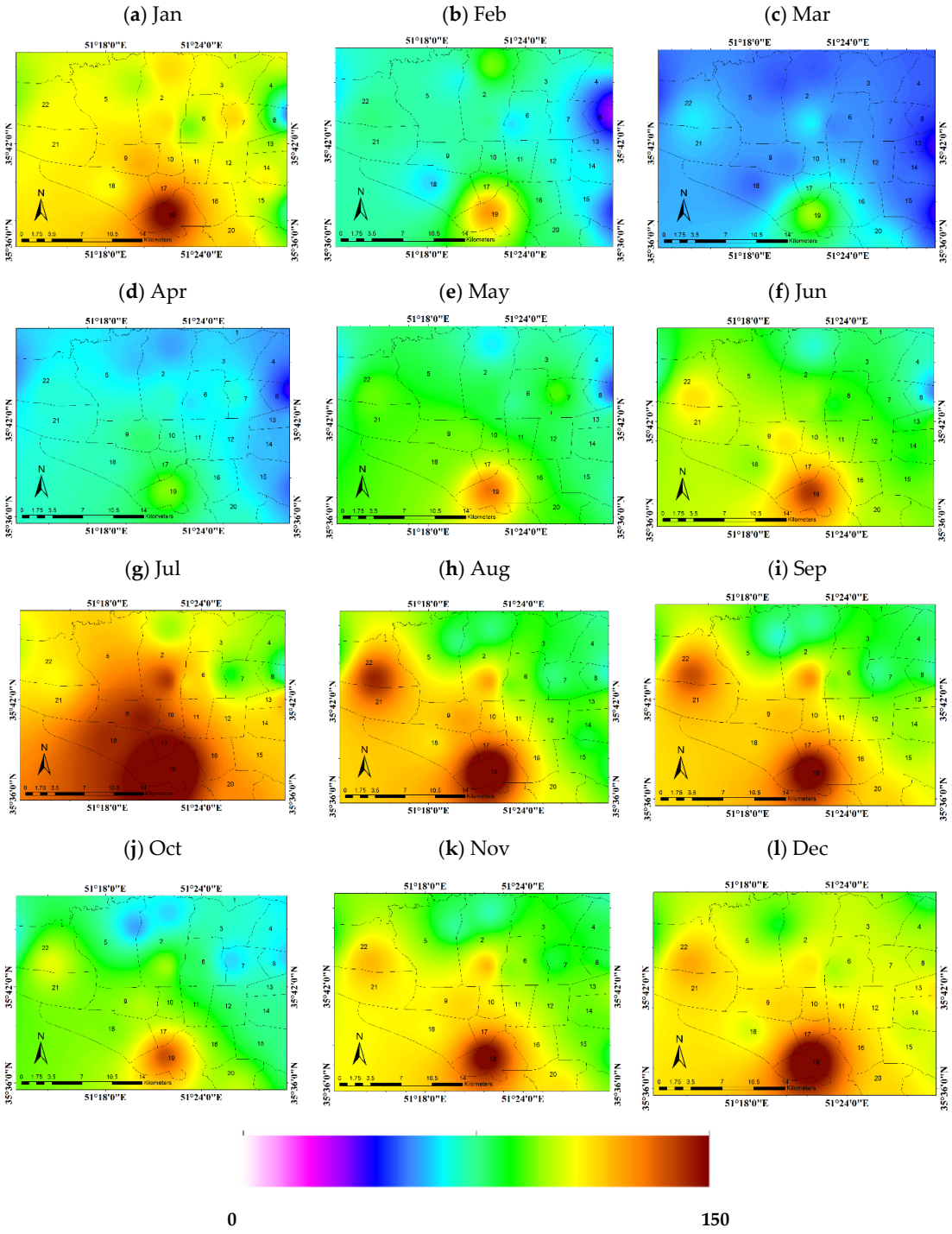

Figure 8. The monthly average concentrations of PM_{10} ($\mu g/m^3$) in Tehran, using data from pollution monitoring stations recorded in 2023.

3.5.2. $PM_{2.5}$ Pollutant

The concentration maps for the monthly average concentration of $PM_{2.5}$ in 2023 in Tehran (Figure 9) shows that the highest $PM_{2.5}$ concentration was recorded in January and December. Increasing the use of fossil fuels for heating and reducing the height of the boundary layer in the cold months of the year are the reasons for this increase in $PM_{2.5}$ concentration [58]. The lowest concentration was observed in April. The dispersion of the areas of maximum concentration of $PM_{2.5}$ was greater than that of PM_{10} in Tehran, and its amount was significant in the south, west, center, and east of Tehran. The $PM_{2.5}$ pattern showed a lot of similarity to the pattern of PM emissions (Figure 8), which indicates that

the amount of this pollutant was higher near its source areas. A review study showed that 85% of previous studies concluded that more than 60% of Tehran air pollution caused by $PM_{2.5}$ comes from mobile sources [59].

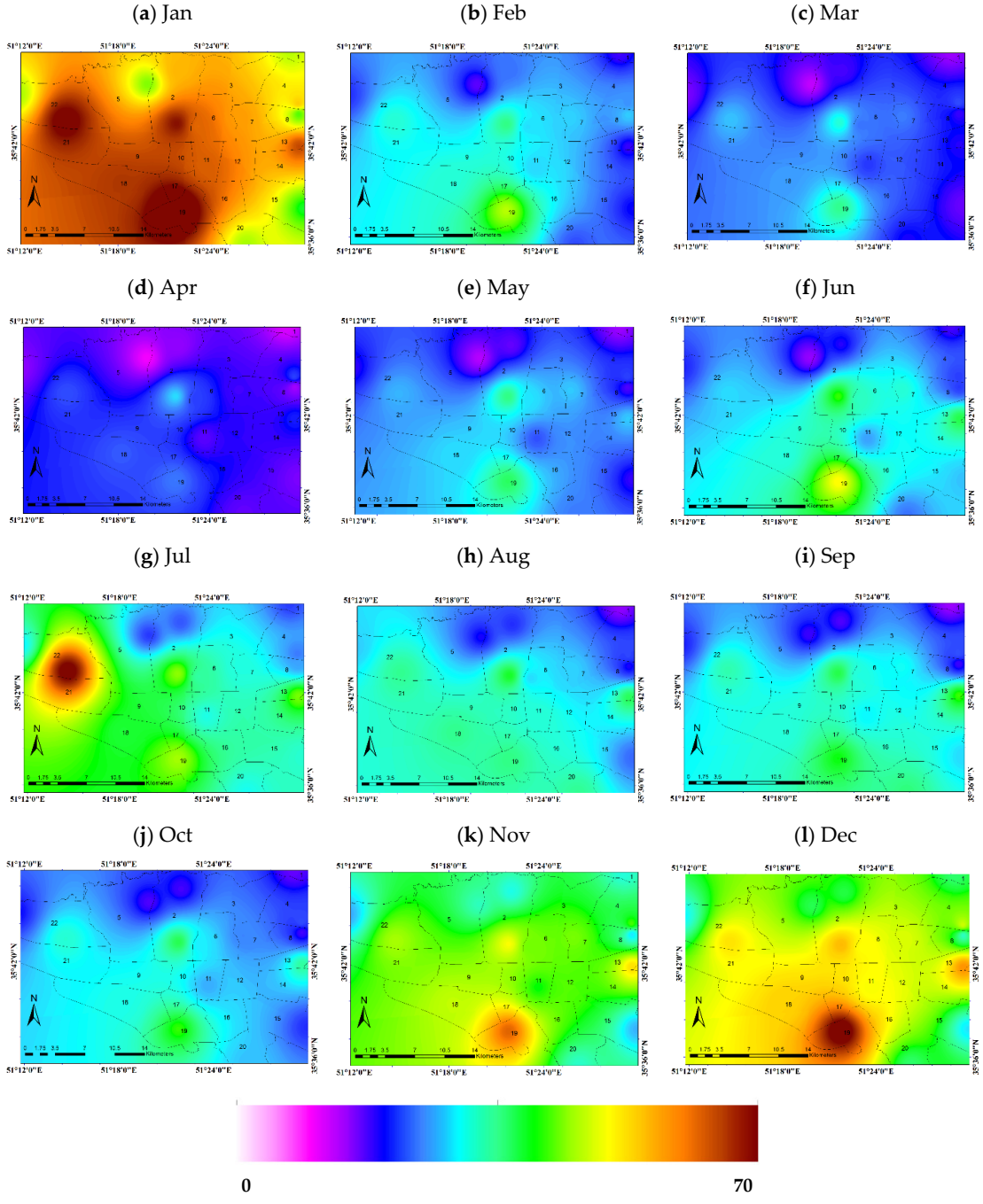

Figure 9. The monthly average concentrations of $PM_{2.5}$ ($\mu g/m^3$) in Tehran, using data from pollution monitoring stations recorded in 2023.

3.5.3. NO_2 Pollutant

Figure 10 shows the monthly average concentrations of NO_2 in Tehran in 2023. The highest concentration was observed in December and January. In general, the concentration of NO_2 in the northeast and north of Tehran was higher than in other regions. Topography is one of the factors affecting the distribution and transmission of air pollution in urban areas [60]. The proximity of northern and northeastern areas of Tehran to the Alborz mountain range is one of the reasons for increasing NO_2 concentration in these areas compared to other parts

of the city. A thermal high-pressure system in mountainous areas, falling cold air, increasing possibility of temperature inversion, and stability of the atmosphere, especially in cold seasons, effectively accumulate pollution in the northern areas of Tehran. Another compelling factor is the wind pattern and the blowing of winds from the plain to the mountains. At the beginning of the morning, the south wind gradually starts blowing from the plain to the mountain (anabatic). During the day, the NO_2 pollutant transfers from the southern parts to the northern parts of the city [61]. Road transportation is the other factor that increases the concentration of NO_2 in the north and northeast of Tehran. The traffic of heavy vehicles to transport goods from factories located in the north of Iran to Tehran, and vice versa, and heavy traffic caused by the transportation of passengers, especially during holidays, increases the amount of NO_2 production in the northern areas of Tehran.

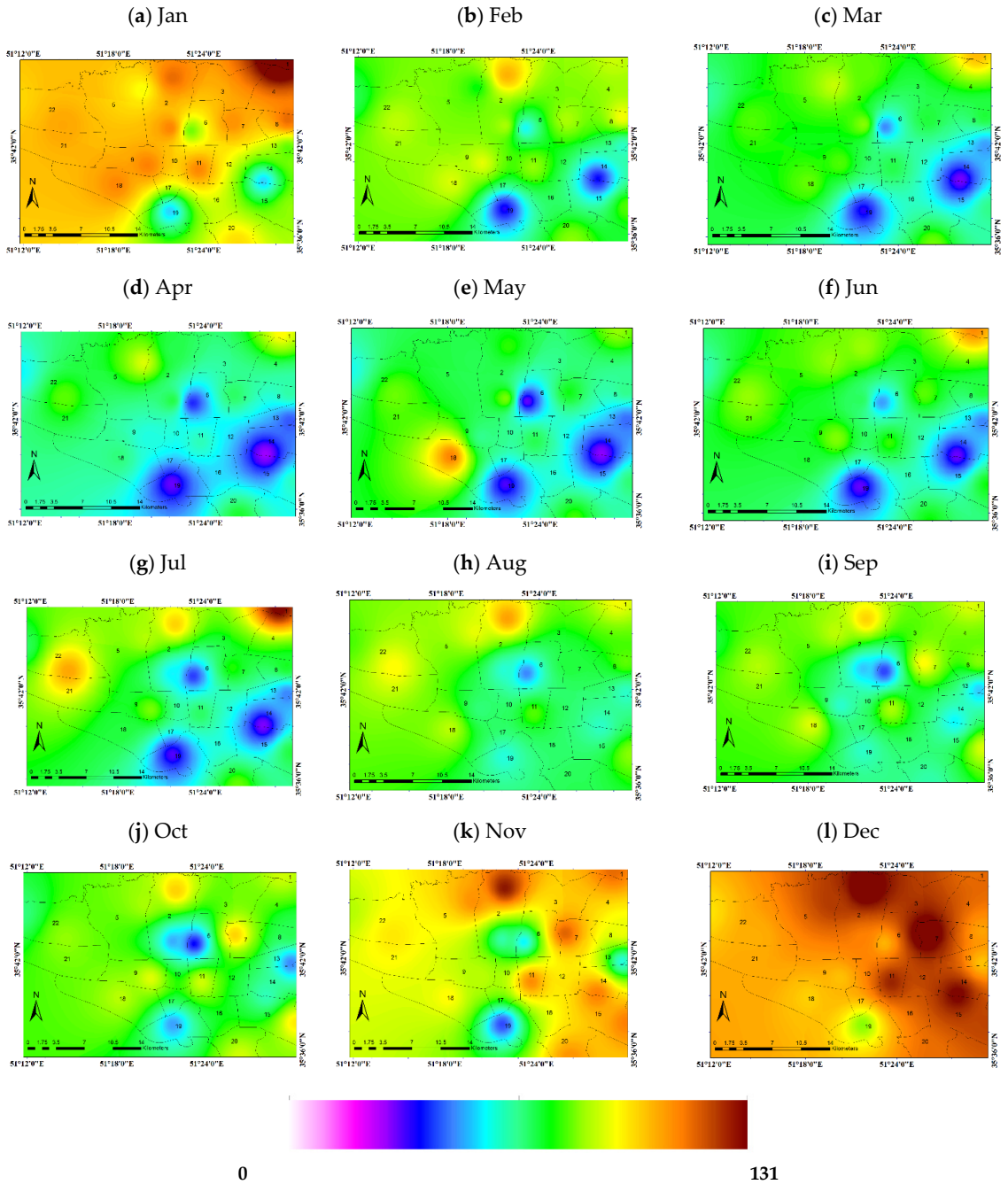

Figure 10. The monthly average concentrations of NO_2 ($\mu g/m^3$) in Tehran, using data from pollution monitoring stations recorded in 2023.

3.6. Investigating the Factors Affecting the Distribution of Pollutants in the TEHRAN Metropolis

Figure 11 shows the annual emission of NO and aerosols in 2013 in Tehran city, on a grid resolution of 500 m (https://air.tehran.ir (accessed on 16 January 2024)). The emission of aerosols in the center, south, and west of Tehran was higher than in the north of the city, but the emission of NO was also significant in the northeast and north of Tehran. In general, the pattern of monthly average concentration of these pollutants in 2023 (Figures 8 and 10) was remarkably similar to their release pattern in 2013.

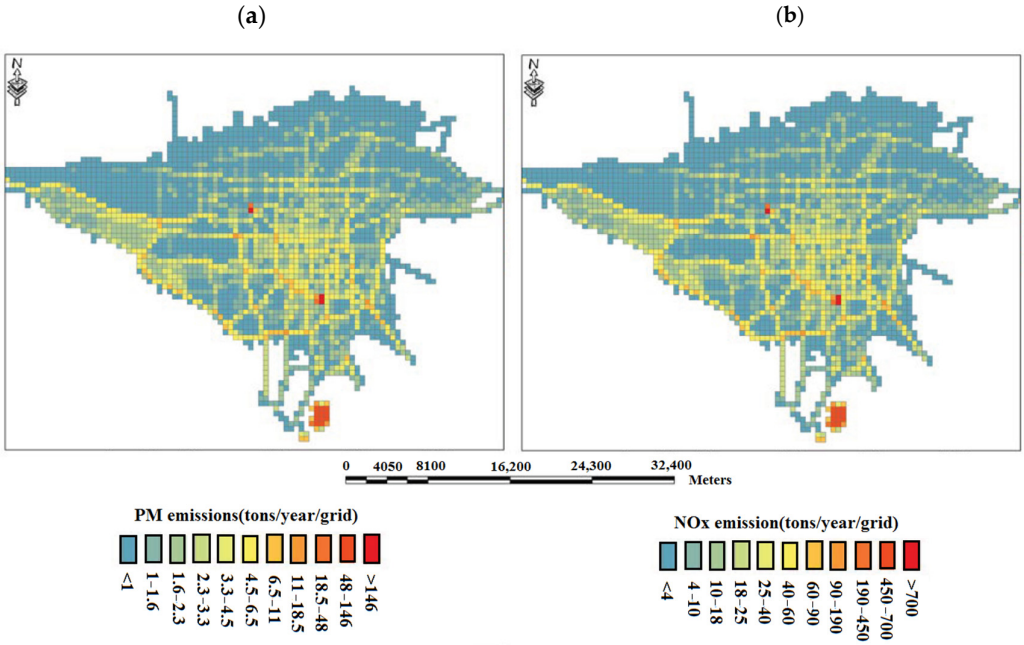

Figure 11. Annual distribution of (**a**) aerosols and (**b**) NO emissions in Tehran city in 2013, https://airnow.tehran.ir (accessed on 13 January 2024).

Correlation coefficients between wind speed, temperature, MSLP, and RH at the Mehrabad station and the concentrations of the NO_2, NO_x, PM_{10}, and $PM_{2.5}$ pollutants at the Shadabad station were calculated for 2023 (Table 4), to determine the effect of atmospheric parameters on pollutant concentrations in Tehran. In general, the correlations were significant for all pollutants, except PM_{10}. This is because the high concentration of PM_{10} is often caused by the influx of dust particles from external areas, which weakens its relationship with atmospheric parameters.

Table 4. Correlations between some atmospheric quantities at Mehrabad station and some pollutants concentration at Shadabad station, 2023.

	NO_2	NO_x	PM_{10}	$PM_{2.5}$
wind	−0.20 **	−0.34 **	−0.02	−0.19 **
temp	−0.26 **	−0.29 **	0.08	−0.45 **
slp	0.28 **	0.30 **	−0.04	0.33 **
RH	0.03	0.18 *	−0.01	0.28 **

* Significant at 5% level. ** Significant at 1% level.

The negative correlation between wind speed and the concentration of all pollutants indicates an inverse relationship: when pollutant concentrations increased, wind speeds tended to be lower. The highest correlation with wind speed was observed for NO_x, followed by NO_2. Temperature also exhibited an inverse relationship with pollutant

concentrations: as pollutant concentrations increased, the temperature was lower. The correlation between $PM_{2.5}$ concentration and temperature was more substantial than for the other pollutants, suggesting a closer association between $PM_{2.5}$ levels and temperature.

The positive correlations between MSLP and pollutant concentrations indicates that air pressure increased when pollutant concentrations were higher. The strongest correlation was observed for $PM_{2.5}$. Furthermore, the correlation between RH and $PM_{2.5}$ was significant at the 1% level, and the correlation with NO_x was significant at the 5% level, but the correlation was not significant for NO_2 or PM_{10} concentrations. The positive correlation coefficients suggest that humidity was higher when the concentrations of these pollutants increased.

3.7. PM_{10} Case Study

3.7.1. July

PM_{10} Concentration

Figure 12 shows the time series of PM_{10} concentration from the Shadabad air pollution monitoring station on 15–19 July 2023, with a 1 h interval. The maximum concentration of PM_{10} at 21 UTC on July 17 was recorded as 1138.9 $\mu g/m^3$. This graph shows a trend of daily changes, so a maximum value is observed every day at the end of the day, when the height of the boundary layer is lower.

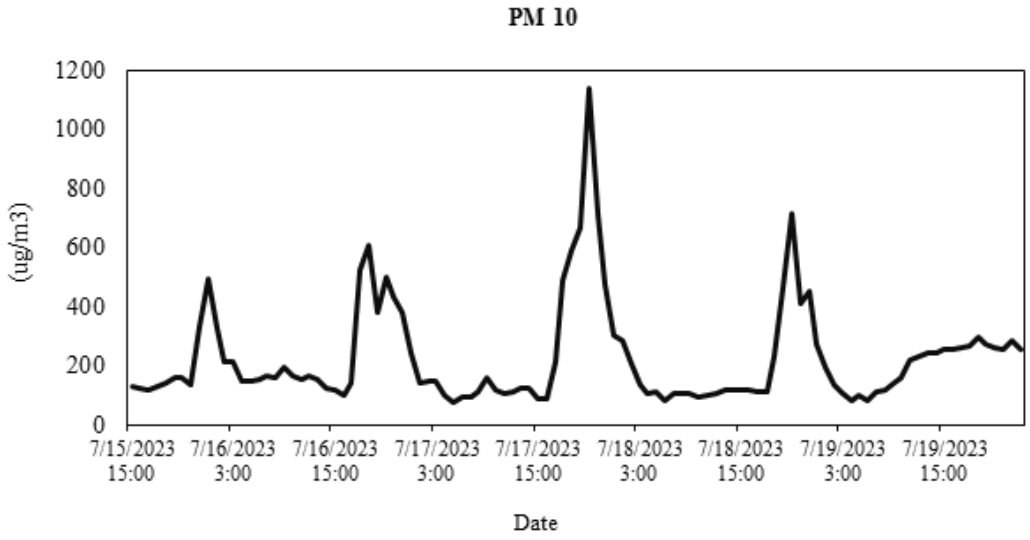

Figure 12. Time series of PM_{10} concentration on 15–19 July 2023.

Figure 13 shows the time series of the concentration of PM_{10}, visibility, and RH on 15–19 July 2023, with a 3 h interval. At 18 UTC on July 16, when the horizontal visibility decreased to 2000 m, the concentration of aerosols increased to 485$\frac{ug}{m^3}$. At this time, there were not any changes in RH, because of the dry air during the warm season in Tehran province.

Synoptic Analysis

On the surface map, a thermal low pressure was observed in the southeast, south, and parts of central Iran, eastern Saudi Arabia, Iraq, eastern Syria, southern Afghanistan, and southwestern Pakistan. The low pressure also influenced the Tehran metropolis. There was a 10 m wind flow in the eastern direction, due to the counter-clockwise circulation of the low pressure towards the study area (Figure 14a). At the level of 850 hPa, a low geopotential height covered the center, south, and southeast of Iran and Pakistan and southern Afghanistan. In Tehran province, the geopotential height was 141 gpm. The wind blew in the southeast direction, with a speed of 10 to 15 m/s, in the southern regions of the province

(Figure 14b). According to the southern dry currents, the RH in Tehran province was less than 30% (Figure 14c). The pattern of 500 hPa geopotential height showed a sub-tropical high over most of the country. In Tehran province, the geopotential height is 578 gpm (Figure 14d).

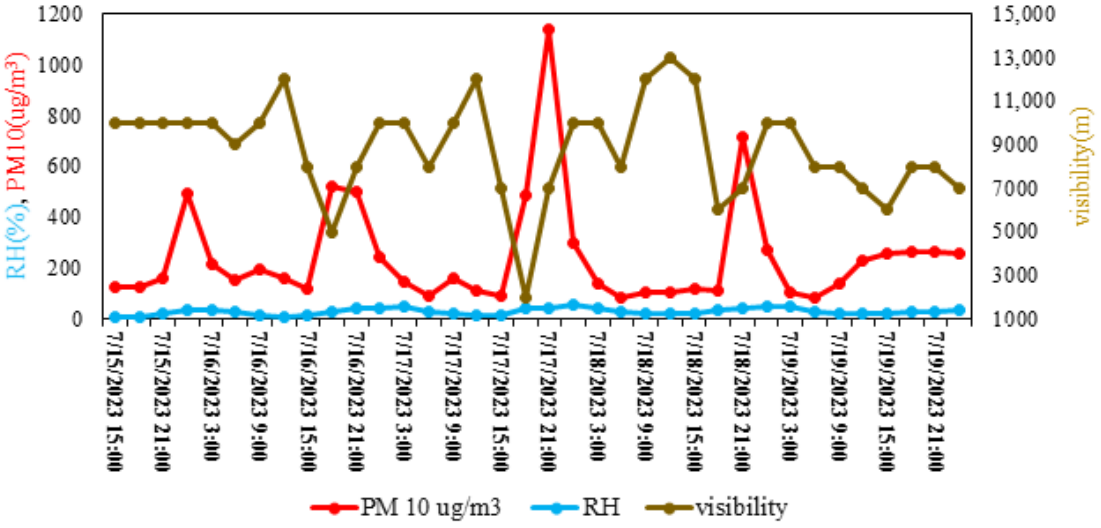

Figure 13. Time series of PM_{10} concentration, visibility, and RH on 15–19 July 2023.

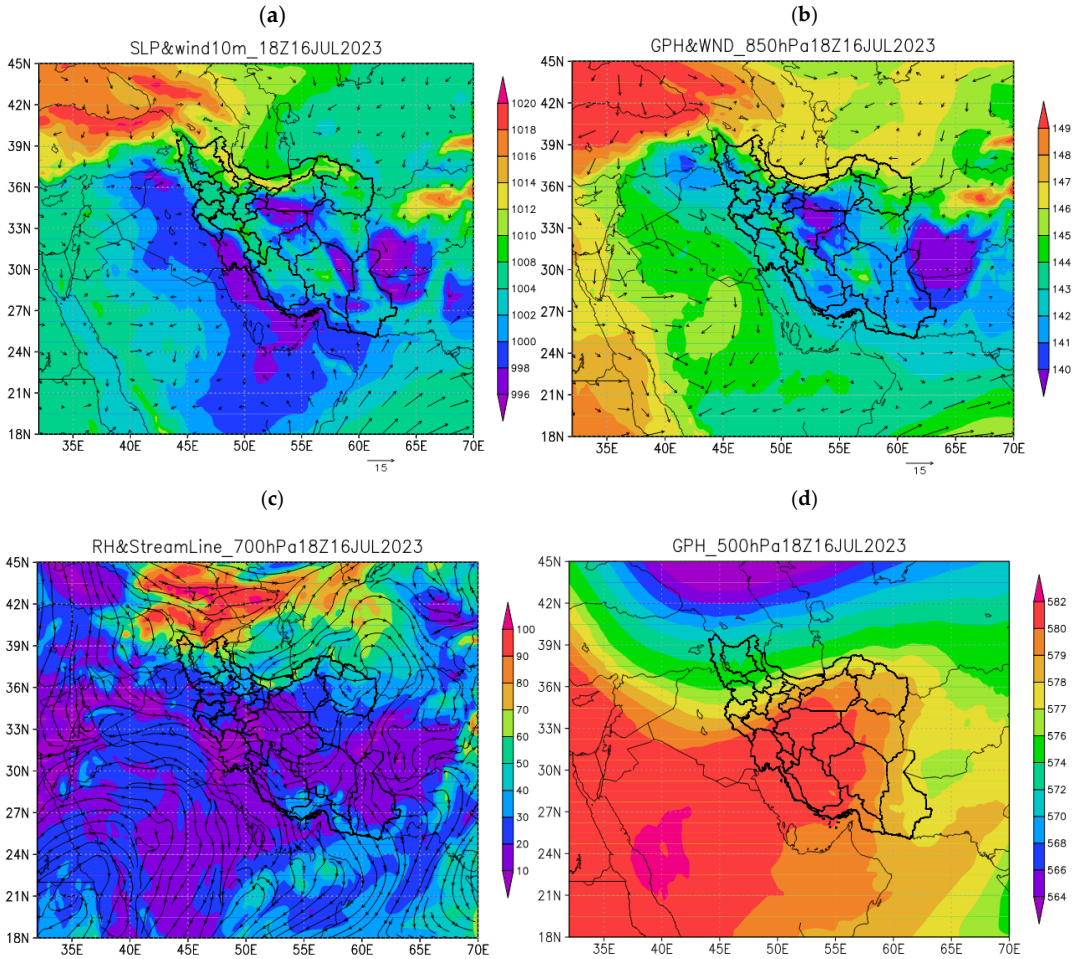

Figure 14. (**a**) MSLP (hPa) and 10 m wind (m/s), (**b**) geopotential height (GPM) and wind speed of 850 hPa (m/s), (**c**) RH (%) and streamline of 700 hPa, and (**d**) geopotential height (GPM) of 500 hPa at 18 UTC on 16 July 2023.

The Skew-T diagram at 00 UTC showed dry air (the temperature diagram and the dew point were away from each other) and a calm wind (Figure 15). In addition, around the level of 870 hPa, a temperature inversion was observed, so the temperature increased slightly with height.

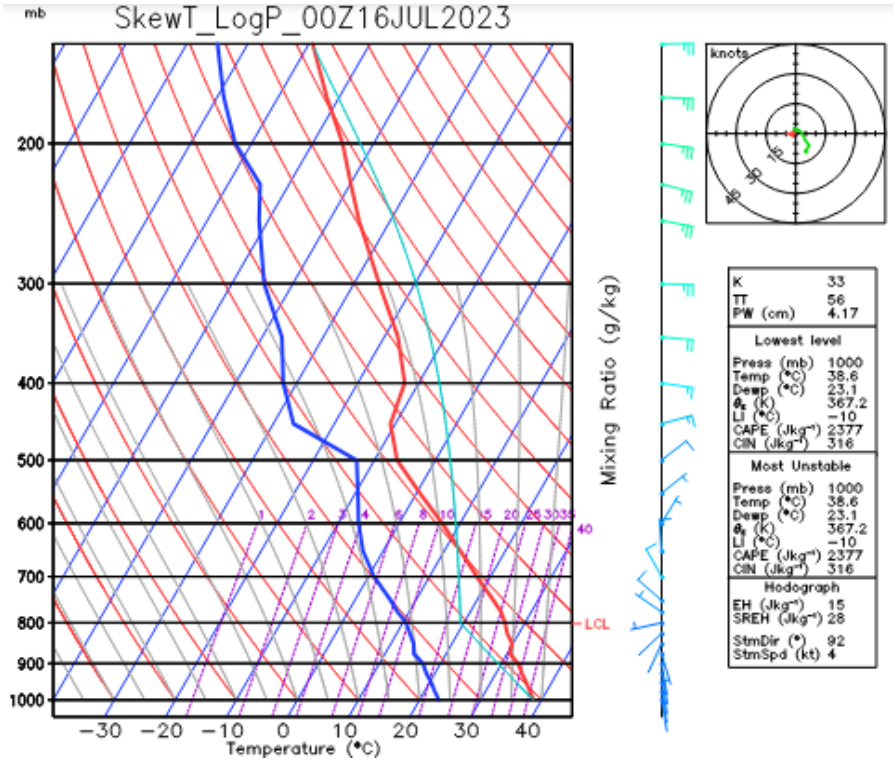

Figure 15. SKEW-T at 00 UTC on 16 July 2023. The red and blue graphs correspond to temperature and dew point temperature, respectively.

Prediction of PM_{10} Pollutant Concentration in Tehran City

Figure 16a shows the concentration of the PM_{10} pollutant at 00 UTC on 18 July 2023, using data from air pollution monitoring stations in Tehran. The PM_{10} concentration output of the 24 h forecast of the CAMS model at the same time is displayed in Figure 16b. The highest concentration of PM_{10} was observed in southern areas of Tehran, which the model predicted correctly. Although the model predicted the pollutant concentration pattern in Tehran correctly to some extent, it underestimated its values, so in order to observe the pollutant concentration pattern in the model output, a different legend was considered.

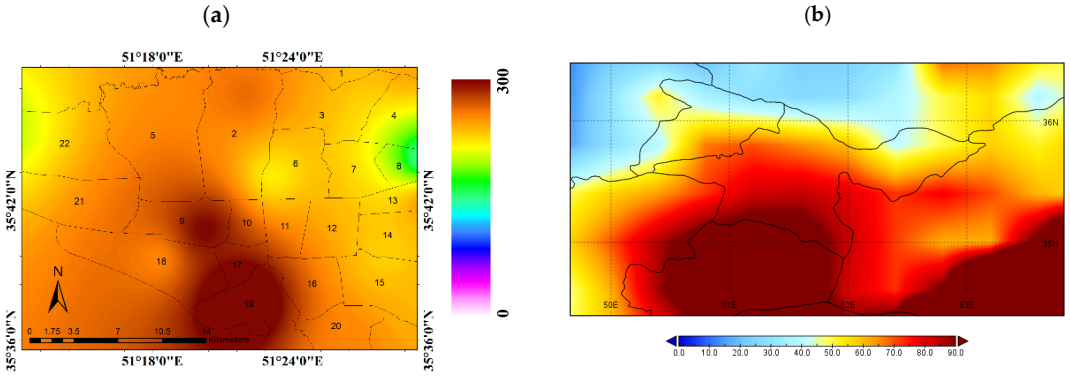

Figure 16. The PM_{10} concentration ($\mu g/m^3$) from (**a**) the air pollution monitoring stations and (**b**) the 24 h forecast of the CAMS model at 00 UTC on 18 July.

3.8. $PM_{2.5}$ Case Study

3.8.1. January

$PM_{2.5}$ Concentration

The time series of the concentration of $PM_{2.5}$ on 1–5 January 2023, with a one-hour interval, is shown in Figure S1. The maximum concentration, 120.8 $\frac{ug}{m^3}$, was observed at 19 UTC on 1 January, followed by 113.3 $\frac{ug}{m^3}$ at 02 UTC on 3 January.

Figure S2 shows the time series of the concentration of $PM_{2.5}$, visibility, and RH on 1–5 January 2023, with a three-hour interval. At 06 UTC on 1 January, as the horizontal visibility decreased to 3500 m, an increasing trend in the concentration of $PM_{2.5}$ was observed, so that the concentration of $PM_{2.5}$ reached 111.1 $\frac{ug}{m^3}$. The RH changed a lot, and its value ranged between 30 and 80%. In this case, the increase in air humidity was associated with a decrease in horizontal visibility and an increase in the concentration of $PM_{2.5}$ aerosols.

Synoptic Analysis

On the surface map, high-pressure centers located east of the Black Sea, and over central and eastern Turkey, northwestern Iran, the Caspian Sea, and its southern coasts, extended to the central parts of Iran and over Syria, Iraq, and the north of Saudi Arabia. The study area was influenced by a high pressure of 1030 hPa, and the 10 m wind blew weakly in the north direction (less than 5 m/s) (Figure S3a). At 850 hPa a, 157 gpm was over the Black Sea, Turkey, and northwest Iran, and extended to Tehran and the center of Iran. A weak, northerly wind blew in Tehran province (Figure S3b). Due to the northerly flow over the Caspian Sea, the northern domains of the Alborz highlands in Mazandaran province had an RH of 50 to 70%, and the southern domains in Tehran province had an RH of 20 to 30% (Figure S3c). The geopotential height pattern of 500 hPa showed a ridge over Saudi Arabia and Iraq. Tehran province had a height of 559 gpm (Figure S3d). At 09 UTC and the hours before, Skew-T showed dry air and calm wind (Figure S4).

Prediction of $PM_{2.5}$ Pollutant Concentration in Tehran City

Figure S5 illustrates the concentration of $PM_{2.5}$ pollutants, using air pollution monitoring data in Tehran and the 24 h forecast of the CAMS model at 00 UTC on 2 January 2023. At this hour, the concentration of $PM_{2.5}$ was high in a large part of Tehran, especially its southern areas, which the model displayed to some extent. In this study, although the model could predict the pollutant concentration pattern, it was still underestimated.

3.9. NO_2 Case Study

3.9.1. December

NO_2 Concentration

The time series of O_3 and NO_2 concentrations from 3 to 7 December 2023, with a one-hour interval, is shown in Figure S6. On the 4th and 5th of December, the NO_2 concentration increased significantly, and its maximum reached more than 250 $\frac{ug}{m^3}$. Comparison of O_3 and NO_2 concentration graphs shows that after the NO_2 concentration reached its maximum amount, the O_3 concentration increased with a time delay (about a few hours), and the NO_2 concentration decreased simultaneously. These conditions correspond to the absorption of sunlight by NO_2 and O_3 formation. On the other hand, the maximum O_3 concentration value was around noon every day.

The time series of NO_2 concentration, horizontal visibility, and RH on 3–6 December 2023, with a three-hour interval, shown in Figure S7, shows that with an increase (decrease) in NO_2 concentration, the horizontal visibility significantly decreased (increased); at 06 UTC on December 4, the horizontal visibility decreased to about 2500 m, and the NO_2 concentration reached about 243 $\frac{ug}{m^3}$ until 06 UTC on December 5. In this period, the RH

had an inverse relationship with horizontal visibility and a direct relationship with NO_2 concentration. Naturally, horizontal visibility decreases with an increase in RH due to the scattering of light by water particles in the atmosphere. The increase in NO_2 concentration simultaneously with an increase in RH is caused by water particles in the atmosphere preventing this pollutant from spreading to higher altitudes and causing it to accumulate near the surface, increasing its surface concentration.

Synoptic Analysis

The surface map shows that the majority of Iran was affected by high pressure. Tehran had a pressure of 1026 hPa, and the wind blew weakly at 10 m (Figure S8a). At the level of 850 hPa, due to the dynamic pattern of the system, there was high geopotential height over Iran, Iraq, and Saudi Arabia; this was also observed in Tehran province (Figure S8b). In Tehran province, the RH was less than 20% (Figure S8c). The geopotential height pattern of 500 hPa showed a ridge over Saudi Arabia to the west of Iran, and another ridge over the southeast to the center of Iran. Tehran province had a height of 570 gpm (Figure S8d). At 06 UTC and in the hours before this, Skew-T showed dry air and calm wind (Figure S9).

Prediction of NO_2 Pollutant Concentration in Tehran City

Figure S10a shows the concentration of NO_2 pollutant at 00 UTC on 5 December 2023, using data from air pollution monitoring stations in Tehran. Simultaneously, the output of the 24 h forecast of NO_2 concentration of the CAMS model is shown in Figure S10b. The concentration of NO_2 at this hour was significant almost all over the city, and its maximum was observed in the northern and central areas of Tehran, which the model predicted almost correctly. In this case, the model underestimated the pollutant concentration, so a different legend was considered to observe the pollutant concentration pattern in the model output.

4. Conclusions

This study examined air pollution in Tehran in 2023, a year with many polluted days, analyzing the relationship between pollutant concentrations and atmospheric factors. Based on the monthly frequency of code 05 at Mehrabad Airport's synoptic station, 72% of haze events occurred in November, December, and January. In nearly all months, the highest haze frequency was recorded at 06 UTC, attributed to increased traffic from school and office openings, temperature inversions, calm winds, and higher humidity during early morning hours. The lowest wind speeds were observed in December, November, and January, correlating with these haze events.

Spatial and temporal patterns of pollutant concentrations in Tehran were also examined using data from monitoring stations. PM_{10} concentrations peaked in July, driven by dust intrusions from local and regional sources. $PM_{2.5}$ concentrations were highest in January and December, influenced by increased fossil fuel use and reduced boundary layer heights in colder months. $PM_{2.5}$'s distribution was more widespread than PM_{10}, with significant levels across the south, west, center, and east of Tehran in many months. NO_2 concentrations peaked in December and January, with higher levels in northern and northeastern Tehran, due to their proximity to the Alborz mountains, which may trap pollutants. Monthly average pollutant patterns closely mirrored emission patterns.

The influence of atmospheric factors on pollutant concentrations was assessed using correlation coefficients between meteorological parameters (wind speed, temperature, MSLP, and RH) at the Mehrabad station and pollutant concentrations (NO_2, NO_x, PM_{10}, and $PM_{2.5}$) at the Shadabad station. Significant correlations were observed for all pollutants, except PM_{10}, as external dust sources often influence its concentrations. Wind speed and temperature showed an inverse relationship with all pollutants. Positive correlations

between MSLP and pollutant concentrations suggested that higher pressures coincided with increased pollution levels. RH had significant positive correlations with $PM_{2.5}$ at the 1% level and with NO_x at the 5% level, indicating higher humidity with increased pollutant concentrations. [40] found that temperature was the primary meteorological factor influencing $PM_{2.5}$ and PM_{10} concentrations. Moderate coupling was also noted between wind speed and NO_2 and CO concentrations.

One case study analyzed the temporal patterns of PM_{10}, $PM_{2.5}$, and NO_2 concentrations, alongside visibility and RH. For $PM_{2.5}$, increases in RH coincided with reduced visibility and higher aerosol concentrations, likely due to hygroscopic particle growth, aerosol formation, and atmospheric stagnation. For NO_2, RH showed an inverse relationship with visibility and a direct relationship with pollutant concentration. The comparison of the pollutant concentration from the CAMS model output with observational data showed that, although the model could predict the pattern of air pollution in Tehran city, it underestimated the values, so quantitative comparison was not possible. The wrong estimation of the pollutant emission inventory is the most possible reason for this error. The complicated topography of Tehran, the small resolution of the CAMS global model, and the error in forecasting weather conditions are among the other reasons that should be analyzed and need more study.

Supplementary Materials: The following supporting information can be downloaded at: https://www.mdpi.com/article/10.3390/atmos16030264/s1, Figure S1: Time series of PM2.5 concentration on January 1–5, 2023; Figure S2: Time series of PM2.5 concentration, visibility and RH on January 1–5, 2023; Figure S3: (a) MSLP and 10-meter wind, (b) geopotential height and wind 850 hPa, (c) RH and streamline 700 hPa and (d) geopotential height of 500 hPa at 09 UTC on January 1, 2023; Figure S4: SKEW-T at 00, 06, 09 and 12 UTC on January 1, 2023; Figure S5: The PM2.5 concentration from (a) air pollution monitoring stations and (b) the 24-hour forecast of the CAMS model, at 00 UTC on January 2, 2023; Figure S6: The time series of ozone and NO_2 concentrations during December 3–7, 2023; Figure S7: The time series of NO_2 concentration, horizontal visibility and RH on December 3–6, 2023; Figure S8: (a) MSLP and 10-meter wind, (b) geopotential height and wind 850 hPa, (c) RH and streamline 700 hPa and (d) geopotential height of 500 hPa at 09 UTC on December 4, 2023; Figure S9: SKEW-T at 00, 06, 12 and 18 UTC on December 4, 2023; Figure S10: The NO2 concentration from (a) air pollution monitoring stations and (b) the 24-hour forecast of the CAMS model, at 00 UTC on December 3, 2023.

Author Contributions: Conceptualization, S.K. and Z.G.; methodology, S.K. and Z.G.; software, S.K. and Z.G.; validation, M.H. and N.K.; formal analysis, S.K. and Z.G.; investigation, M.H.; resources, M.H.; data curation, S.K., Z.G. and N.K.; writing—original draft preparation, S.K. and Z.G.; writing—review and editing, M.H.; visualization, S.K. and Z.G.; supervision, M.H. and N.K.; project administration, S.K. and Z.G.; funding acquisition, M.H. All authors have read and agreed to the published version of the manuscript.

Funding: Open Access Funding by the University of Graz.

Institutional Review Board Statement: Not applicable.

Informed Consent Statement: Not applicable.

Data Availability Statement: The original contributions presented in this study are included in the article/Supplementary Material. Further inquiries can be directed to the corresponding author(s).

Acknowledgments: The authors thank the Copernicus teams for the ERA5 reanalysis data providing the meteorological maps. We are also thankful for Tehran air pollution data retrieval via the Tehran Air Quality Control Company website, affiliated with the Tehran Municipality (https://airnow.tehran.ir (accessed on 13 January 2024)). IRIMO is acknowledged for its valuable Data Archive of Synoptic stations in Tehran. Finally, the authors express their gratitude to the ECMWF team for providing informative products for the CAMS model forecast. Open Access Funding by the University of Graz.

Conflicts of Interest: The authors declare that there is no conflict of interests regarding the publication of this manuscript. In addition, ethical issues, including plagiarism, informed consent, misconduct, data fabrication and/or falsification, double publication and/or submission, and redundancy, have been completely observed by the authors.

References

1. Anwar, M.N.; Shabbir, M.; Tahir, E.; Iftikhar, M.; Saif, H.; Tahir, A.; Murtaza, M.A.; Khokhar, M.F.; Rehan, M.; Aghbashlo, M.; et al. Emerging challenges of air pollution and particulate matter in China, India, and Pakistan and mitigating solutions. *J. Hazard. Mater.* **2021**, *416*, 125851. [CrossRef] [PubMed]
2. Zhang, X.; Han, L.; Wei, H.; Tan, X.; Zhou, W.; Li, W.; Qian, Y. Linking urbanization and air quality together: A review and a perspective on the future sustainable urban development. *J. Clean. Prod.* **2022**, *346*, 130988. [CrossRef]
3. Guo, Q.; He, Z.; Wang, Z. Change in air quality during 2014–2021 in Jinan city in China and its influencing factors. *Toxics* **2023**, *11*, 210. [CrossRef] [PubMed]
4. Shahriyari, H.A.; Nikmanesh, Y.; Jalali, S.; Tahery, N.; Zhiani Fard, A.; Hatamzadeh, N.; Zarea, K.; Cheraghi, M.; Mohammadi, M.J. Air pollution and human health risks: Mechanisms and clinical manifestations of cardiovascular and respiratory diseases. *Toxin Rev.* **2022**, *41*, 606–617. [CrossRef]
5. Sierra-Vargas, M.P.; Montero-Vargas, J.M.; Debray-García, Y.; Vizuet-de-Rueda, J.C.; Loaeza-Román, A.; Terán, L.M. Oxidative stress and air pollution: Its impact on chronic respiratory diseases. *Int. J. Mol. Sci.* **2023**, *24*, 853. [CrossRef] [PubMed]
6. Maio, S.; Sarno, G.; Tagliaferro, S.; Pirona, F.; Stanisci, I.; Baldacci, S.; Viegi, G. Outdoor air pollution and respiratory health. *Int. J. Tuberc. Lung Dis.* **2023**, *27*, 7–12. [CrossRef] [PubMed]
7. Gholami, S.; Behnami, A.; Benis, K.Z. Air Pollution and Cancer. In *Diseases and Health Consequences of Air Pollution*; Academic Press: Cambridge, MA, USA, 2024; pp. 85–108.
8. Alahmad, B.; Khraishah, H.; Althalji, K.; Borchert, W.; Al-Mulla, F.; Koutrakis, P. Connections between air pollution, climate change, and cardiovascular health. *Can. J. Cardiol.* **2023**, *39*, 1182–1190. [CrossRef]
9. Fowler, D.; Brimblecombe, P.; Burrows, J.; Heal, M.R.; Grennfelt, P.; Stevenson, D.S.; Jowett, A.; Nemitz, E.; Coyle, M.; Liu, X.; et al. A chronology of global air quality. *Philos. Trans. R. Soc. A* **2020**, *378*, 20190314. [CrossRef]
10. Haywood, J. Atmospheric Aerosols and Their Role in Climate Change. In *Climate Change*; Elsevier: Amsterdam, The Netherlands, 2021; pp. 645–659.
11. Chen, Y.; Haywood, J.; Wang, Y.; Malavelle, F.; Jordan, G.; Peace, A.; Partridge, D.G.; Cho, N.; Oreopoulos, L.; Grosvenor, D.; et al. Substantial cooling effect from aerosol-induced increase in tropical marine cloud cover. *Nat. Geosci.* **2024**, *17*, 404–410. [CrossRef]
12. Mahowald, N.M.; Li, L.; Albani, S.; Hamilton, D.S.; Kok, J.F. Opinion: The importance of historical and paleoclimate aerosol radiative effects. *Atmos. Chem. Phys.* **2024**, *24*, 533–551. [CrossRef]
13. Esteban-Cantillo, O.J.; Menendez, B.; Quesada, B. Climate change and air pollution impacts on cultural heritage building materials in Europe and Mexico. *Sci. Total Environ.* **2024**, *921*, 170945. [CrossRef] [PubMed]
14. Guo, Q.; He, Z.; Wang, Z. The Characteristics of Air Quality Changes in Hohhot City in China and their Relationship with Meteorological and Socio-economic Factors. *Aerosol Air Qual. Res.* **2024**, *24*, 230274. [CrossRef]
15. Liu, Y.; Zhou, Y.; Lu, J. Exploring the relationship between air pollution and meteorological conditions in China under environmental governance. *Sci. Rep.* **2020**, *10*, 14518. [CrossRef] [PubMed]
16. Chen, J.; Liu, Z.; Yin, Z.; Liu, X.; Li, X.; Yin, L.; Zheng, W. Predict the effect of meteorological factors on haze using BP neural network. *Urban Clim.* **2023**, *51*, 101630. [CrossRef]
17. Chen, Z.; Chen, D.; Zhao, C.; Kwan, M.P.; Cai, J.; Zhuang, Y.; Zhao, B.; Wang, X.; Chen, B.; Yang, J.; et al. Influence of meteorological conditions on PM2. 5 concentrations across China: A review of methodology and mechanism. *Environ. Int.* **2020**, *139*, 105558. [CrossRef] [PubMed]
18. Guo, Q.; He, Z.; Li, S.; Li, X.; Meng, J.; Hou, Z.; Liu, J.; Chen, Y. Air pollution forecasting using artificial and wavelet neural networks with meteorological conditions. *Aerosol Air Qual. Res.* **2020**, *20*, 1429–1439. [CrossRef]
19. Al-Hemoud, A.; Al-Sudairawi, M.; Al-Rashidi, M.; Behbehani, W.; Al-Khayat, A. Temperature inversion and mixing height: Critical indicators for air pollution in hot arid climate. *Nat. Hazards* **2019**, *97*, 139–155. [CrossRef]
20. Yavuz, V. An analysis of atmospheric stability indices and parameters under air pollution conditions. *Environ. Monit. Assess.* **2023**, *195*, 934. [CrossRef] [PubMed]
21. Ngangmo, Y.C.; Adiang, C.M.; Choudhary, A.; Monkam, D. Road traffic-induced particle matter dispersion in a calm wind environment at the main roundabout in Douala, central Africa. *J. Air Pollut. Health* **2023**, *8*, 59–76. [CrossRef]
22. Zhu, T.; Tang, M.; Gao, M.; Bi, X.; Cao, J.; Che, H.; Chen, J.; Ding, A.; Fu, P.; Gao, J.; et al. Recent progress in atmospheric chemistry research in China: Establishing a theoretical framework for the "Air Pollution Complex". *Adv. Atmos. Sci.* **2023**, *40*, 1339–1361. [CrossRef] [PubMed]

23. Shi, Z.; Vu, T.; Kotthaus, S.; Harrison, R.M.; Grimmond, S.; Yue, S.; Zhu, T.; Lee, J.; Han, Y.; Demuzere, M.; et al. Introduction to the special issue "In-depth study of air pollution sources and processes within Beijing and its surrounding region (APHH-Beijing)". *Atmos. Chem. Phys.* **2019**, *19*, 7519–7546. [CrossRef]
24. Guo, Q.; He, Z.; Wang, Z. Prediction of hourly PM2. 5 and PM10 concentrations in Chongqing City in China based on artificial neural network. *Aerosol Air Qual. Res.* **2023**, *23*, 220448. [CrossRef]
25. Shu, L.; Xie, M.; Gao, D.; Wang, T.; Fang, D.; Liu, Q.; Huang, A.; Peng, L. Regional severe particle pollution and its association with synoptic weather patterns in the Yangtze River Delta region, China. *Atmos. Chem. Phys.* **2017**, *17*, 12871–12891. [CrossRef]
26. Qian, W.; Xu, M.; Ai, Y. Anomaly-based synoptic analysis to identify and predict meteorological conditions of strong ozone events in North China. *Air Qual. Atmos. Health* **2022**, *15*, 1699–1711. [CrossRef]
27. He, Z.; Guo, Q. Comparative Analysis of Multiple Deep Learning Models for Forecasting Monthly Ambient PM2. 5 Concentrations: A Case Study in Dezhou City, China. *Atmosphere* **2024**, *15*, 1432. [CrossRef]
28. Guo, Q.; He, Z.; Wang, Z. Predicting of daily PM2. 5 concentration employing wavelet artificial neural networks based on meteorological elements in Shanghai, China. *Toxics* **2023**, *11*, 51. [CrossRef]
29. He, Z.; Guo, Q.; Wang, Z.; Li, X. Prediction of monthly PM2. 5 concentration in Liaocheng in China employing artificial neural network. *Atmosphere* **2022**, *13*, 1221. [CrossRef]
30. Appel, K.W.; Bash, J.O.; Fahey, K.M.; Foley, K.M.; Gilliam, R.C.; Hogrefe, C.; Hutzell, W.T.; Kang, D.; Mathur, R.; Murphy, B.N.; et al. The Community Multiscale Air Quality (CMAQ) model versions 5.3 and 5.3. 1: System updates and evaluation. *Geosci. Model Dev. Discuss.* **2020**, *2020*, 1–41. [CrossRef]
31. Tessum, C.W.; Hill, J.D.; Marshall, J.D. InMAP: A model for air pollution interventions. *PLoS ONE* **2017**, *12*, e0176131. [CrossRef]
32. Dimov, I.; Georgiev, K.; Ostromsky, T.; Zlatev, Z. Computational challenges in the numerical treatment of large air pollution models. *Ecol. Model.* **2004**, *179*, 187–203. [CrossRef]
33. Berrocal, V.J.; Gelfand, A.E.; Holland, D.M. Space-time data fusion under error in computer model output: An application to modeling air quality. *Biometrics* **2012**, *68*, 837–848. [CrossRef] [PubMed]
34. Ghorani-Azam, A.; Riahi-Zanjani, B.; Balali-Mood, M. Effects of air pollution on human health and practical measures for prevention in Iran. *J. Res. Med. Sci.* **2016**, *21*, 65.
35. Saniei, R.; Zangiabadi, A.; Sharifikia, M.; Ghavidel, Y. Air quality classification and its temporal trend in Tehran, Iran, 2002–2012. *Geospat. Health* **2016**, *11*, 2. [CrossRef] [PubMed]
36. Faraji, A.; Mortazavi, M.; Hamidizadeh, A. Systematic analysis of primary and secondary mechanisms affecting air pollution in Tehran. *J. Clim. Res.* **2022**, *1401*, 183–200.
37. Thanvisitthpon, N.; Kallawicha, K.; Chao, H.J. Effects of Urbanization and Industrialization on Air Quality. In *Health and Environmental Effects of Ambient Air Pollution*; Academic Press: Cambridge, MA, USA, 2024; pp. 231–255.
38. Hadian, M.; Raeissi, P.; Harati Khalilabad, T. The economic burden of mortality and morbidity due to air pollution in Tehran, Iran: A systematic review. *Air Qual. Atmos. Health* **2020**, *13*, 1001–1011. [CrossRef]
39. Torbatian, S.; Hoshyaripour, A.; Shahbazi, H.; Hosseini, V. Air pollution trends in Tehran and their anthropogenic drivers. *Atmos. Pollut. Res.* **2020**, *11*, 429–442. [CrossRef]
40. Yousefian, F.; Faridi, S.; Azimi, F.; Aghaei, M.; Shamsipour, M.; Yaghmaeian, K.; Hassanvand, M.S. Temporal variations of ambient air pollutants and meteorological influences on their concentrations in Tehran during 2012–2017. *Sci. Rep.* **2020**, *10*, 292. [CrossRef] [PubMed]
41. ShahMohammadi, M.; Bay, Y.; Kiani, P.A.R.V.A.N.E.H. Identifying and Prioritizing the Factors Affecting Air Pollution in Tehran with an Interpretive Structural Modeling Approach. *Environ. Interdiscip. Dev.* **2022**, *7*, 88–98.
42. Talkhabi, H.; Jafarpour Ghalehteimouri, K.; Toulabi Nejad, M. Integrating Tehran metropolitan air pollution into the current transport system and sprawl growth: An emphasis on urban performance and accessibility. *Discov. Cities* **2024**, *1*, 1–13. [CrossRef]
43. Inness, A.; Ades, M.; Agustí-Panareda, A.; Barré, J.; Benedictow, A.; Blechschmidt, A.M.; Dominguez, J.J.; Engelen, R.; Eskes, H.; Flemming, J.; et al. The CAMS reanalysis of atmospheric composition. *Atmos. Chem. Phys.* **2019**, *19*, 3515–3556. [CrossRef]
44. Khansalari, S.; Fazel-Rastgar, F.; Mohammadi, L.M.; Gozalkhoo, M. Clustering of different atmospheric patterns leading to an increase in different types of atmospheric pollutants in the greater Tehran area during the last 17 years (2004–2020). *J. Air Pollut. Health* **2021**, *6*, 54–71. [CrossRef]
45. Pegahfar, N.; Bidokhti, A.A.; Zawar-Reza, P.; Farahani, M.M. Study of vertical wind profiles in an urban area with complex terrain (Tehran). *J. Earth Syst. Sci.* **2011**, *120*, 825–841. [CrossRef]
46. Xiang, Y.; Zhang, T.; Liu, J.; Lv, L.; Dong, Y.; Chen, Z. Atmosphere boundary layer height and its effect on air pollutants in Beijing during winter heavy pollution. *Atmos. Res.* **2019**, *215*, 305–316. [CrossRef]
47. Wang, M.; Tang, G.; Liu, Y.; Ma, M.; Yu, M.; Hu, B.; Zhang, Y.; Wang, Y.; Wang, Y. The difference in the boundary layer height between urban and suburban areas in Beijing and its implications for air pollution. *Atmos. Environ.* **2021**, *260*, 118552. [CrossRef]
48. Su, T.; Li, Z.; Kahn, R. Relationships between the planetary boundary layer height and surface pollutants derived from lidar observations over China: Regional pattern and influencing factors. *Atmos. Chem. Phys.* **2018**, *18*, 15921–15935. [CrossRef]

49. Crosbie, E.; Sorooshian, A.; Monfared, N.A.; Shingler, T.; Esmaili, O. A multi-year aerosol characterization for the greater Tehran area using satellite, surface, and modeling data. *Atmosphere* **2014**, *5*, 178–197. [CrossRef] [PubMed]
50. Shi, Y.; Liu, L.; Hu, F.; Fan, G.; Huo, J. Nocturnal Boundary Layer Evolution and Its Impacts on the Vertical Distributions of Pollutant Particulate Matter. *Atmosphere* **2021**, *12*, 610. [CrossRef]
51. Majumder, A.K.; Rahman, M.; Patoary, M.N.A.; Kamruzzaman, A.M.; Majumder, R. Time Series Analysis PM2● 5 Concentration for Capital City Dhaka from 2016 to 2023. *Science* **2024**, *5*, 35–42.
52. Sun, Y.; Song, T.; Tang, G.; Wang, Y. The vertical distribution of PM2. 5 and boundary-layer structure during summer haze in Beijing. *Atmos. Environ.* **2013**, *74*, 413–421. [CrossRef]
53. Mao, J.; Bali, K.; Campbell, J.R.; Robinson, E.S.; DeCarlo, P.F.; Ijaz, A.; Temime-Roussel, B.; Ketcherside, D.; Yokelson, R.J.; Hu, L.; et al. Multiphase sulfur chemistry facilitates particle growth in a cold and dark urban environment. *Faraday Discuss.* **2024**. [CrossRef]
54. Kermani, M.; Jonidi Jafari, A.; Gholami, M.; Arfaeinia, H.; Shahsavani, A.; Fanaei, F. Characterization, possible sources and health risk assessment of PM2. 5-bound Heavy Metals in the most industrial city of Iran. *J. Environ. Health Sci. Eng.* **2021**, *19*, 151–163. [CrossRef]
55. Nguyen, D.H.; Lin, C.; Vu, C.T.; Cheruiyot, N.K.; Nguyen, M.K.; Le, T.H.; Lukkhasorn, W.; Bui, X.T. Tropospheric ozone and NO_x: A review of worldwide variation and meteorological influences. *Environ. Technol. Innov.* **2022**, *28*, 102809. [CrossRef]
56. Farahani, V.J.; Arhami, M. Contribution of Iraqi and Syrian dust storms on particulate matter concentration during a dust storm episode in receptor cities: Case study of Tehran. *Atmos. Environ.* **2020**, *222*, 117163. [CrossRef]
57. Namdari, S.; Karimi, N.; Sorooshian, A.; Mohammadi, G.; Sehatkashani, S. Impacts of climate and synoptic fluctuations on dust storm activity over the Middle East. *Atmos. Environ.* **2018**, *173*, 265–276. [CrossRef]
58. Fuladlu, K.; Altan, H. Examining land surface temperature and relations with the major air pollutants: A remote sensing research in case of Tehran. *Urban Clim.* **2021**, *39*, 100958. [CrossRef]
59. Khajehpour, H.; Taksibi, F.; Hassanvand, M.S. Comparative review of ambient air PM2. 5 source apportioning studies in Tehran. *J. Environ. Health Sci. Eng.* **2023**, *21*, 21–34. [CrossRef]
60. Afarideh, F.; Ramasht, M.H.; Mortyn, G. Air pollution and topography in Tehran. *AUC Geogr.* **2023**, *58*, 157–171. [CrossRef]
61. Bidokhti, A.A.; Shariepour, Z.; Sehatkashani, S. Some resilient aspects of urban areas to air pollution and climate change, case study: Tehran, Iran. *Sci. Iranica. Trans. A Civ. Eng.* **2016**, *23*, 1994.

Disclaimer/Publisher's Note: The statements, opinions and data contained in all publications are solely those of the individual author(s) and contributor(s) and not of MDPI and/or the editor(s). MDPI and/or the editor(s) disclaim responsibility for any injury to people or property resulting from any ideas, methods, instructions or products referred to in the content.